Environmental Science and Pollution Research (2024) 31:48014–48026
https://doi.org/10.1007/s11356-024-33959-7

RESEARCH ARTICLE

Preparation of catalyst for CO_2 hydrogenation reaction based on the idea of element sharing and preliminary exploration of catalytic mechanism

He Jia[1] · Tao Du[1,2,3] · Yingnan Li[1] · Heming Wang[1] · Qiang Yue[1] · Lifeng Zhou[1] · Yisong Wang[1]

Received: 18 March 2024 / Accepted: 6 June 2024 / Published online: 17 July 2024

Abstract

Under the background of the continuous rise of CO_2 annual emissions, the development of CO_2 capture and utilization technology is urgent. This study focuses on improving the catalytic capacity of the catalyst for CO_2 hydrogenation, improving the efficiency of CO_2 conversion to methanol, and converting H_2 into chemical substances to avoid the danger of H_2 storage. Based on the concept of element sharing, the ASMZ (Aluminum Shares Metal Zeolite catalysts) series catalyst was prepared by combining the CuO–ZnO–Al_2O_3 catalyst with the ZSM-5 zeolite using the amphoteric metal properties of the Al element. The basic structural properties of ASMZ catalysts were compared by XRD, FTIR, and BET characterization. Catalytic properties of samples were measured on a micro fixed-bed reactor. The catalytic mechanism of the catalyst was further analyzed by SEM, TEM, XPS, H_2-TPR, and NH_3-TPD. The results show that the ASMZ3 catalyst had the highest CO_2 conversion rate (26.4%), the highest methanol selectivity (76.0%), and the lowest CO selectivity (15.3%) in this study. This is mainly due to the fact that the preparation method in this study promotes the exposure of effective weakly acidic sites and medium strength acidic sites (facilitating the hydrogenation of CO_2 to methanol). At the same time, the close binding of Cu–ZnO–Al_2O_3 (CZA) and ZSM-5 zeolite also ensures the timely transfer of catalytic products and ensures the timely play of various catalytic active centers. The preparation method of the catalyst in this study also provides ideas for the preparation of other catalysts.

Keywords CO_2 hydrogenation · Micro fixed-bed reactor · ASMZ catalyst · Methanol · Acidic sites · Catalytic mechanism

Introduction

According to carbon dioxide (CO_2) emissions data published by the International Energy Agency (IEA), global CO_2 emissions from energy combustion and industrial processes increased by 0.9% in 2022 from the previous year, reaching a record high of 36.8 billion tonnes (energy agency 2022). These CO_2 emissions are attributed to energy combustion. Therefore, the further conversion of CO_2 into energy substances and the realization of CO_2 circular economy can effectively avoid CO_2 emissions caused by energy combustion. The continued growth of global CO_2 emissions means that the goal of peaking CO_2 emissions has not yet been achieved, and technologies for reducing CO_2 emissions still need to be further developed. China has also proposed to achieve "carbon peak" by 2030 and "carbon neutrality" by 2060. China's Carbon Dioxide Capture, Utilization and Storage (CCUS) Annual Report (2023) points out that CCUS technology can achieve large-scale sustainable low-carbon use of fossil energy, help build a low-carbon industrial system, and is an indispensable part of China's carbon neutral technology system (Zhang et al. 2023). CO_2 hydrogenation utilization technology can convert CO_2 into energy substances to reduce CO_2 emissions, while converting H_2

Responsible Editor: George Z. Kyzas

✉ Tao Du
dut@smm.neu.edu.cn

[1] State Environmental Protection Key Laboratory of Eco-Industry, Northeastern University, Shenyang 110819, China

[2] National Frontiers Science Center for Industrial Intelligence and Systems Optimization, Northeastern University, Shenyang 110819, China

[3] Key Laboratory of Data Analytics and Optimization for Smart Industry (Northeastern University), Ministry of Education, Shenyang, China

into chemical substances, avoiding the danger of H_2 storage (Fang et al. 2023). Therefore, this study focuses on catalysts for the reaction of CO_2 and H_2.

In recent years, in the field of CO_2 hydrogenation, scientists have carried out a lot of research. The reaction products of CO_2 and H_2 include methane (Ding et al. 2024), methanol (Chen et al. 2024b), dimethyl ether (Li et al. 2023), olefin (Wang et al. 2024), aromatics (Chen et al. 2024a), gasoline (Ahmed et al. 2023), etc. Among them, methanol can be used as a raw material for the synthesis of high-grade chemicals and an ideal hydrogen source to replace high-pressure hydrogen in hydrogenation reactions (Chen et al. 2023). In recent years, researchers have been working on catalysts that can promote the conversion of CO_2 to methanol under milder conditions (Sun et al. 2023). Through a large number of experiments and mechanism studies, the researchers found that the synergistic interaction between the active component of the catalyst and the carrier has an important effect on the performance of the catalyst, including porosity, surface area (Ren et al. 2020), metal-carrier interaction (Yang et al. 2021b), metal particle size, metal dispersion (Wang et al. 2022), oxygen vacancy (Zhang et al. 2022), chemical composition reduction (Singh et al. 2022), pH value, etc. Ren et al. (Ren et al. 2019) changed the specific surface area and porosity of the CuO–ZnO–Al_2O_3 catalyst by controlling the concentration of metal ions in the reaction solution. It was found that catalysts with high specific surface area and Cu surface area had higher CO_2 conversion. Chen et al. (Chen et al. 2022) prepared Cu/ZnO/ZrO_2 catalysts with flower, plate, and rod-like ZnO morphologies by the urea hydrolysis method and used them for CO_2 hydrogenation to methanol. The results of performance test showed that the methanol yield increased linearly with the increase of oxygen vacancy concentration, indicating that oxygen vacancy played an important role in the process of CO_2 hydrogenation to methanol. Guo et al. (Guo et al. 2021) prepared Cu–ZnO/Al_2O_3–ZrO_2 (CZAZ) mesostructural catalyst and optimized the microstructure and surface properties of the catalyst. It was found that the homogeneous mesoporous structure and the strong interaction between Cu and support made the CZAZ-8 catalyst have higher metal Cu-active surface area and more Cu-CO_2 adsorption sites, which promoted the CO_2 conversion. Qi et al. (Qi et al. 2021) synthesized Cu/ZnO/Y_2O_3 ternary catalyst using citric acid coordination assisted strategy. It is found that the enhanced activity of the Cu/ZnO/Y_2O_3 catalyst for methanol synthesis is related to the small size of the Cu/ZnO/Y_2O_3 catalyst, highly dispersed Cu species, abundant surface adsorption sites, and more strong interaction between Cu–ZnO interfaces. However, how to carefully control and modify these structural properties at the same time in order to accelerate the catalytic process, improve mass transfer, increase the number of active sites, and improve the efficiency of the reaction pathway still needs further research. Based on the above research status, this study innovatively proposed a new method of linking metal oxide catalyst with zeolite carrier, which realized the wide distribution of active components, the full exposure of weak and medium strong acidic sites, and greatly promoted the CO_2 conversion efficiency of CO_2 hydrogenation reaction and the selectivity of product CH_3OH.

In this study, based on the concept of element sharing, we combined the CuO–ZnO–Al_2O_3 catalyst with the ZSM-5 zeolite to prepare ASMZ series catalysts by utilizing the amphoteric metal characteristics of the Al element. Using Al in the CuO–ZnO–Al_2O_3 catalyst as an aluminum source, ASMZ catalysts with different Si/Al ratios were prepared, and their properties were tested and characterized. In order to explore the catalytic mechanism of ASMZ series catalysts, XPS, H_2-TPR, CO_2-TPD, and other tests were carried out to reveal the mechanism of high CO_2 conversion and high CH_3OH selectivity of the ASMZ3 catalyst.

Experimental

Sample preparation

Copper nitrate, zinc nitrate, aluminum nitrate, ammonium nitrate, sodium bicarbonate, tetrapropyl ammonium hydroxide (TPAOH, 25 wt.% in H_2O), sodium chloride, and tetraethyl orthosilicate (TEOS) were purchased from Sinopharm.

The CuO–ZnO–Al_2O_3 catalyst was prepared by a reverse co-precipitation method named as CZAB (Wang et al. 2011). The molar ratio of Cu/Zn/Al was 6/3/1. The ZSM-5 zeolite was synthesized by a hydrothermal method (Wan et al. 2016). In particular, CZAB was used as an aluminum source to achieve aluminum sharing. TEOS was used as a silicon source. Samples with different Si/Al ratios (12.5, 25, 37.5, and 50) were hydrothermally reacted at 453 K and calcined at 823 K to remove TPAOH. Ion exchange was then performed to replace Na^+ with NH_4^+ by mixing 1.0 g of every sample in 50 mL of 1.0 M NH_4Cl solution at 323 K for 8 h. The procedure was repeated twice to ensure complete ion exchange. The ion-exchanged samples were again collected by centrifugation and washed in deionized water three times, dried at 373 K overnight, and calcined at 773 K for 5 h to obtain the final H^+ type ZSM-5 samples. Finally, all the samples were reduced under H_2/Ar (5% H_2) atmosphere for 4 h with the temperature of 573 K. The obtained samples were aluminum shared metal zeolite catalysts named ASMZ1, ASMZ2, ZSMZ3, and ASMZ4. The CZAB sample was reduced under the same conditions and named CZA. The approximate process is shown in Fig. 1.

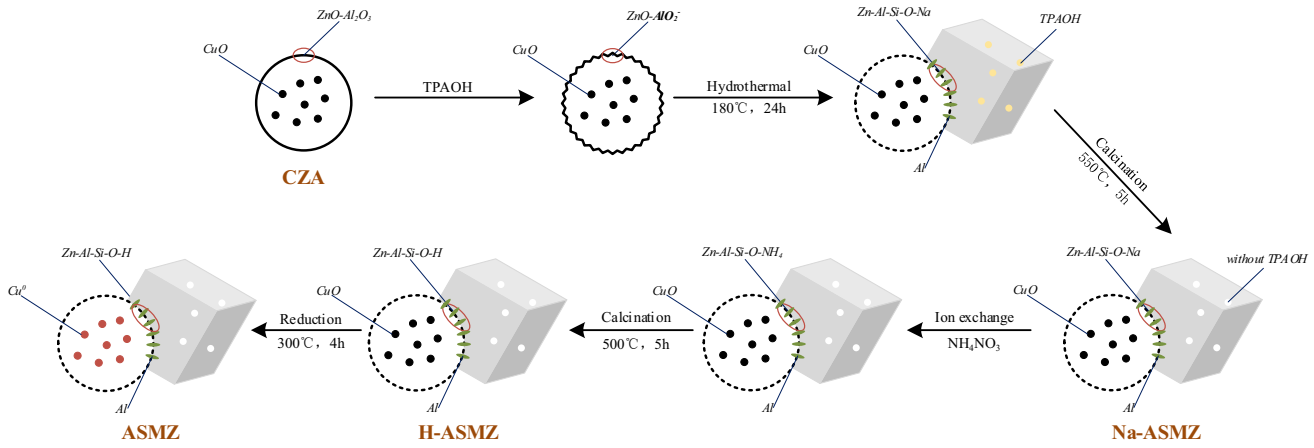

Fig. 1 Schematic diagram of the synthesis process

Characterization methods

The crystal structure of samples was measured by a powder X-ray diffractometer (D8 ADVANCE, Bruker) equipped with a Cu anticathode. The measuring range was from 5 to 80° with a step of 0.02°. The skeleton structure of samples was measured by a Fourier infrared spectrometer (Cary 660 FTIR, Agilent). All the samples had been dried at 393 K overnight before measured and a measuring range of 500~4000 cm^{-1}. The nitrogen adsorption/desorption isotherms of the samples were recorded using a physical adsorption apparatus (ASAP 2460, Micromeritics) at 77 K. The pretreatment condition of the samples was vacuum drying at 573 K for 6 h. The Brunauer-Emmett-Teller (BET) and T-plot models were used to analyze the specific surface area, pore size distribution, and the micropore volume. The chemical composition of samples was performed by X-ray fluorescence (XRF) with a ZSX Primus ii spectrometer (Rigaku, Japan). The microcrystal morphology of samples was observed by a scanning electron microscope (GeminiSEM 300, ZEISS). The crystal lattice structure of samples was further observed by transmission electron microscopy (F200X, FEI Talos). Elemental mapping of samples was conducted using energy dispersive X-ray spectroscopy (EDS super-X) to describe the elemental distributions. Elemental distribution and valence states for each sample were analyzed by ex situ X-ray photoelectron spectroscopy (XPS, Thermo Scientific K-Alpha) with Al Kα ($h\nu$ = 1486.6 eV) radiation. The samples were reduced by H_2 prior to analyses, and the C1 s (284.8 eV) was used as reference for the calibration of binding energies.

To test the reducibility of the samples, hydrogen temperature programed reduction (H_2-TPR) was conducted on a chemisorbed instrument (BSD-Chem C200) equipped with a thermal conductivity detector (TCD). Prior to the test, the sample was purged by argon at 473 K for 2 h to baseline stabilization aiming at removing moisture and absorbed water. The temperature of the sample was then cooled to 323 K. Finally, the sample was heated from 323 to 1073 K (with a ramp rate of 5 K min^{-1}) in 5% H_2 flow (balanced with Ar), during which the H_2 consumption was measured by the TCD. The surface acidity determination of samples was tested by NH_3 temperature programmed desorption (NH_3-TPD). Weigh 0.1 g of the reduced sample and place it in a U-shaped quartz tube, program the temperature at 10 K min^{-1} from room temperature to 573 K for drying and pretreatment, purge with He gas (30 mL min^{-1}) for 1 h, naturally cool to 393 K, and add 10% NH_3 (balanced with He) gas (30 mL min^{-1}) for 1 h. After the baseline is stable, switch to 30 mL/min He gas, increase to 873 K at a heating rate of 5 K min^{-1} for desorption, and use online mass spectrometry to detect the desorbed gas.

Performance testing

Catalytic properties of samples were measured on a micro fixed-bed reactor reported in our previous work. The schematic diagram of the reactor is shown in Fig. S1. In order to avoid the reaction gas ratio deviation caused by the reaction pressure building process, the feedstock gas was directly selected H_2/CO_2 (3:1) mixture. The reaction temperature (523 K) and pressure (3 MPa) were controlled by the three-stage furnace and backpressure regulator, respectively. Products were online monitored by the gas chromatograph (GC, GC-102, Henven) equipped with a thermal conductivity detector (TCD) and a flame ionization detector (FID), and the outlet flowrate was measured by a digital bubble flowmeter.

In a typical measurement, 1 g of catalyst (50~70 mesh) was uniformly mixed with equal volume quartz sand (50~70 mesh) and together installed in the center of the

reaction column. Then, the inlet gas was premixed gas of H_2 and CO_2 with the flowrate of 25 NmL min^{-1}.

The CO_2 conversion (%) was calculated as

$$X_{CO_2} = \frac{F_{in} \times P_{CO_2,in} - F_{out} \times P_{CO_2,out}}{F_{in} \times P_{CO_2,in}} \times 100\%$$

where F_{in} (mL min^{-1}) was the inlet flowrate, $P_{CO2,in}$ (%) was the molar fraction of CO_2 in the inlet, F_{out} (mL min^{-1}) was the outlet flowrate, and $P_{CO2,out}$ (%) was the molar fraction of CO_2 in the outlet.

The selectivity of product (%) was calculated as

$$S_i = \frac{F_{out} \times P_{i,out} \times C_i}{F_{in} \times P_{CO_2,in} - F_{out} \times P_{CO_2,out}}$$

where i was the product of CO, MeOH, or DME. $P_{i,out}$ (%) was the molar fraction of product i in the outlet. C_i was the carbon number of product i.

The yield (%) of product i was calculated as

$$Y_i = X_{CO_2} \times S_i \times 100\%$$

where i was the product, viz., MeOH + DME, CO, etc.

The space-time yield (g kg_{cat}^{-1} h^{-1}) on the unit mass of the catalyst of product i was calculated as

$$STY_i = \frac{F_{in} \times P_{CO_2,in} \times X_{CO_2} \times S_i \times M_i \times 60}{m_{cat} \times 22.4}$$

where i was the product, viz., MeOH + DME, CO, etc. M_i (g/mol) was the mole weight of product i. m_{cat} (g) was the mass of the catalyst.

Only methanol, DME, and CO were detected in products, and the carbon balance was confirmed before and after reactions (within 100 ± 2%).

Results and discussion

Catalyst structure study

In order to confirm the crystal structure of the samples, XRD characterization analysis was performed on them. The results are presented in Fig. 2a. It is found that all ASMZ samples contain both the crystallization peaks of ZSM-5 zeolite (ICDD PDF No.44-0003) and elemental copper (ICDD PDF No.85-1326). The XRD patterns (Fig. S2) of the pre-reduction catalysts (named ASMZ1-B, ASMZ2-B, ASMZ3-B, and ASMZ4-B) were compared. It was found that the structure of the ZSM-5 zeolite was not destroyed by the reduction treatment and CuO was fully reduced. The relative intensity change trend of the characteristic peak of the Cu element is consistent with the feeding amount. XRD analysis results verify that the crystal structure of the samples is in line with expectations.

In order to test the skeleton structure of the ASMZ samples, they were characterized by FTIR and presented in Fig. 2b. The transmission peaks observed at ~3130 cm^{-1} and ~1400 cm^{-1} are relating to the stretching vibration of O–H bond, which results from the physically adsorbed water. The overlapped peaks of Cu–O bond, Zn–O bond, and Al–O bond are observed at the wavenumber of ~500 cm^{-1} (Zhao et al. 2020). To ASMZ catalysts, the main vibration frequency peaks at ~1225, ~1100, ~800, ~550, and ~450 cm^{-1} can be identified, corresponding to the characteristic of MFI type zeolites (Jia et al. 2021). The transmission peak intensity of the MFI zeolite structure increases with the increase of the Si/Al ratio, and the intensities of ASMZ3 and ASMZ4 are similar, further verifying that the MFI structure of the ASMZ3 and ASMZ4 catalysts is more complete.

In order to further analyze the internal pore structure of the catalysts, the N_2 adsorption-desorption isotherm (Fig. 2c) was tested at 77 K, and calculated and analyzed

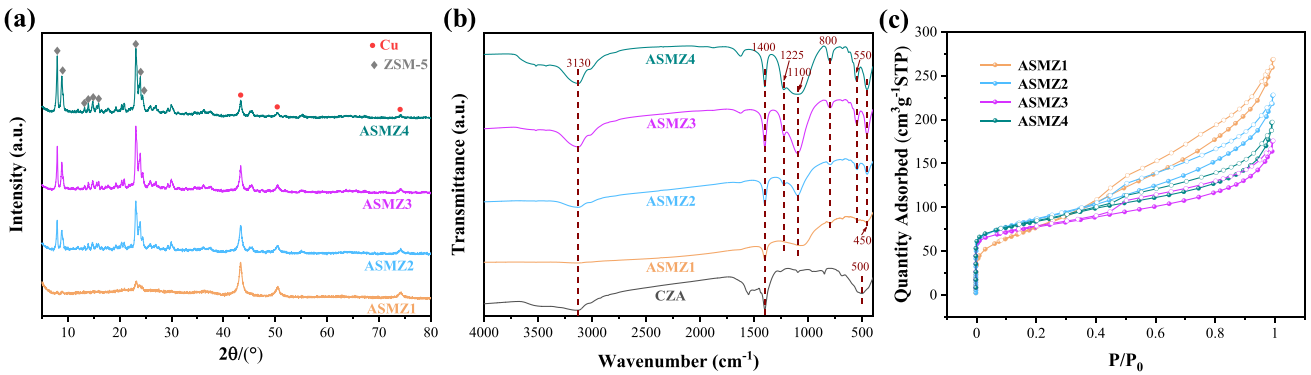

Fig. 2 Structural characterization of catalysts. a XRD patterns of ASMZ and CZA catalysts; b FTIR spectra of ASMZ and CZA catalysts; c N_2 adsorption-desorption isotherms of ASMZ catalysts

by the 2D-NLDFT model. The results are listed in Table 1. Among all the catalysts, ASMZ3 has the lowest specific surface area, but its micropore volume and the ratio of micropores to the total pore volume are the highest. Besides, the micropore area increases with the increase of the Si/Al ratio. It shows that the zeolite microporous structure of ASMZ3 and ASMZ4 is more abundant in catalysts per unit mass.

Table 1 Textural properties of ASMZ catalysts

Samples	S_{BET} (m^2/g)	t-Plot S_{Micro} (m^2/g)	V_{total} (cm^3/g)	$V_{micropore}$ (cm^3/g)	$R_{micropore}$ (%)
CZA	35.9	0.0	0.180	0.000	0.0
ASMZ1	282.0	0.0	0.414	0.000	0.0
ASMZ2	289.4	94.4	0.353	0.049	13.9
ASMZ3	252.8	116.0	0.272	0.061	22.4
ASMZ4	276.8	117.6	0.305	0.061	20.0

S_{BET} = BET surface area, which was calculated using the BET method; t-Plot S_{Micro} = micropore area, which was determined using the t-plot method

Catalysis in CO_2 hydrogenation

Fig. 3 shows the performance of catalysts in CO_2 hydrogenation with a feed gas at a typical reaction condition (the pressure of 3 MPa and temperature of 523 K) containing CO_2 and H_2 (H_2:CO_2 = 3:1). Meanwhile, Fig. 3a shows the CO_2 conversion rate of the samples and the selectivity of each product; Fig. 3b shows the yield of each product and the proportional relationship between the yield of MeOH and DME and the yield of CO; Figure 3c shows the space-time yield

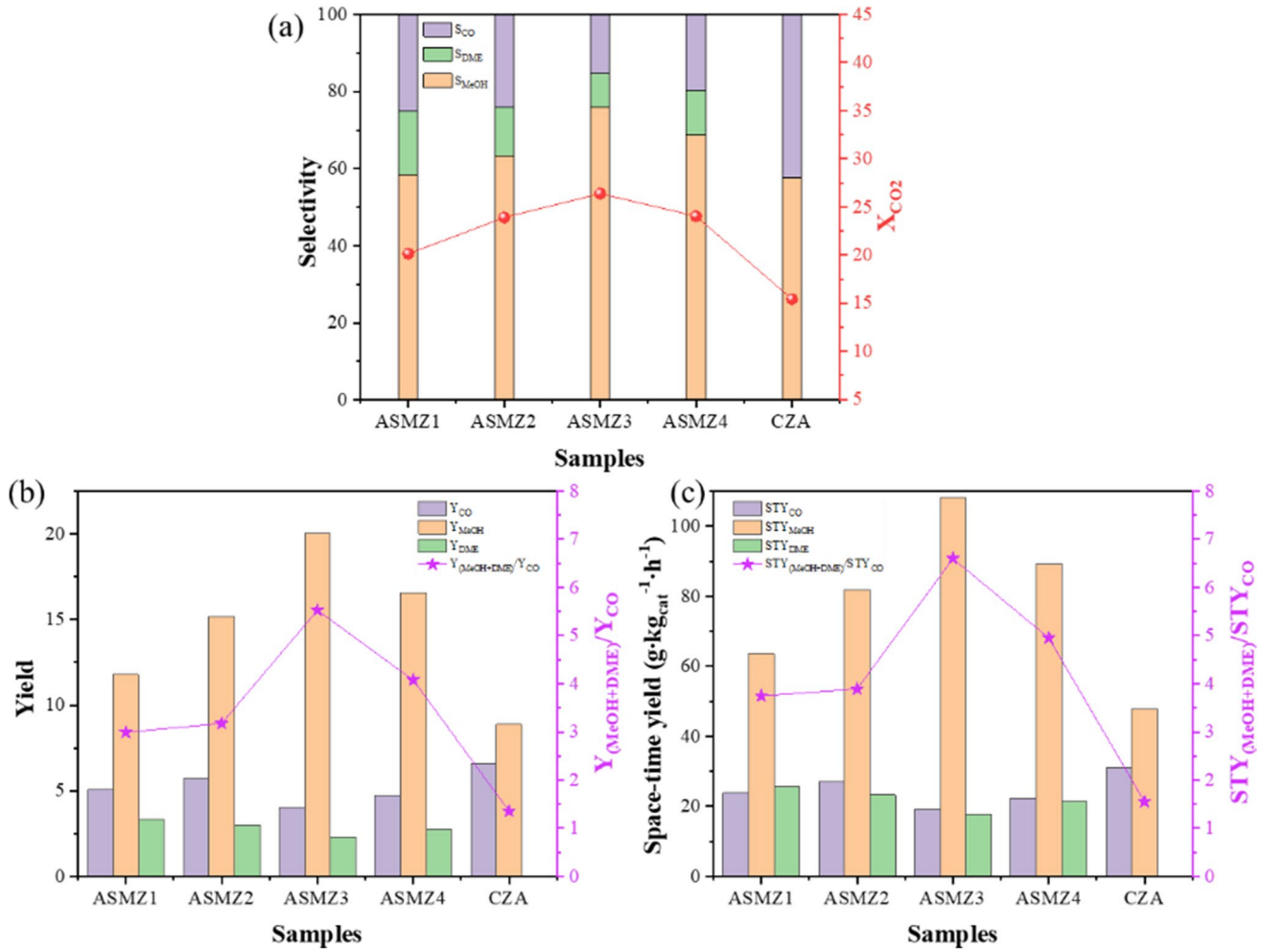

Fig. 3 Performance of ASMZ and CZA catalysts in CO_2 hydrogenation: a CO_2 conversion of catalysts and selectivity of different products; b the yield of the different catalytic products and the ratio of the yield of the target products (methanol and DME, $Y_{(MeOH + DME)}$) to the yield of the by-product (CO, Y_{CO}); c the space-time yield of different catalytic products and the ratio of the space-time yield of the target products (methanol and DME, $STY_{(MeOH + DME)}$) to the space-time yield of the by-product (CO, STY_{CO}). (Reaction conditions: 1 g of catalyst, 3 MPa, 523 K, H_2:CO_2 = 3:1, GHSV = 1500 mL g^{-1} h^{-1})

of each product and the proportional relationship between the space-time yield of MeOH and DME and the space-time yield of CO. Detailed data are shown in Table 2. According to the results, CZA could only convert CO_2 into methanol and CO with the CO_2 conversion of 15.4% and CO selectivity of 42.5%. The yield of MeOH was only 8.9%, and the space-time yield of MeOH was only 47.9 g kg_{cat}^{-1} h^{-1}. On the contrary, the catalyst after combining CZA and ZSM-5 zeolite through the sharing of the aluminum element significantly increased the CO_2 conversion and reduced the CO selectivity under the same reaction conditions. Among them, the sample with the best catalytic performance, ASMZ3, had a CO_2 conversion as high as 26.4%, and a CO selectivity as low as 15.3%. The yield and space-time yield of MeOH were as high as 20.0% and 108.1 g kg_{cat}^{-1} h^{-1} respectively. The proportional relationship between $STY_{(MeOH + DME)}$ and STY_{CO} of ASMZ3 was high to 6.6, which was much higher than that of CZA ($STY_{(MeOH + DME)}/STY_{CO} = 1.5$). It can be speculated that the addition and dosage ratio of the ZSM-5 zeolite had a significant effect on the catalytic performance of the samples.

Mechanism study

Morphology and element distribution analysis

In order to study the effect mechanism of the ZSM-5 zeolite on the catalytic performance, the samples were characterized by SEM, TEM, and XPS. Fig. 4 shows the SEM images of catalysts ASMZ1, ASMZ2, ASMZ3, and ASMZ4. According to the analysis of the characterization results, the particle size of the ZSM-5 zeolite in the catalysts was about 1 μm, except for ASMZ1 which was about 2 μm. The large walnut-shaped particle in the picture was the ZSM-5 zeolite, and the small particle attached to it was the catalytic active component CZA. This could also be demonstrated by analyzing the SEM line scan test results of catalyst ASMZ4 (Fig. S3). Through the partial magnification, it could be observed that the CZA particles were closely connected with the ZSM-5 particles instead of wrapped inside ZSM-5. With the increase of Si/Al, the coverage area of CZA gradually decreased, and the dispersion became better and better. At the same time, the proportion of active ingredient CZA was also less and less.

In order to further observe the internal structure and element distribution of ASMZ catalysts, individual particles of each catalyst were selected and subjected to face scanning of all elements. Fig. 5 shows TEM and surface

Table 2 Catalytic property of ASMZ and CZA catalysts

Samples	X_{CO2} (%)	Selectivity (%)			Yield (%)			Space-time yield (g kg_{cat}^{-1} h^{-1})$_e$		
		MeOH	DME	CO	MeOH	DME	CO	MeOH	DME	CO
CZA	15.4	57.5	0.0	42.5	8.9	0.0	6.6	47.9	0.0	30.9
ASMZ1	20.1	58.5	16.4	25.1	11.8	3.3	5.0	63.6	25.6	23.8
ASMZ2	23.9	63.4	12.6	24.0	15.2	3.0	5.7	81.8	23.3	27.0
ASMZ3	26.4	76.0	8.7	15.3	20.1	2.3	4.0	108.1	17.8	19.1
ASMZ4	24.0	68.8	11.4	19.8	16.6	2.7	4.7	89.3	21.3	22.3

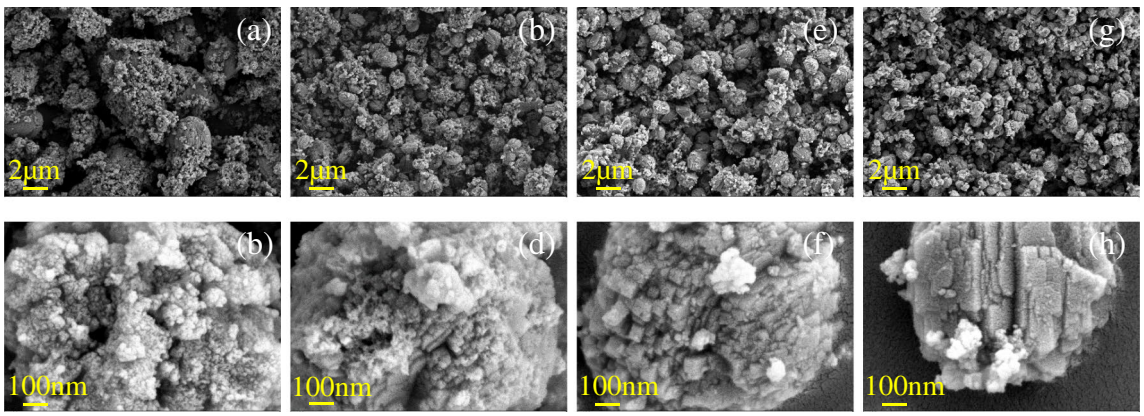

Fig. 4 SEM images of ASMZ catalysts at different magnifications. **a** ASMZ1; **b** ASMZ1; **c**, **d** ASMZ2; **e**, **f** ASMZ3; **g**, **h** ASMZ4

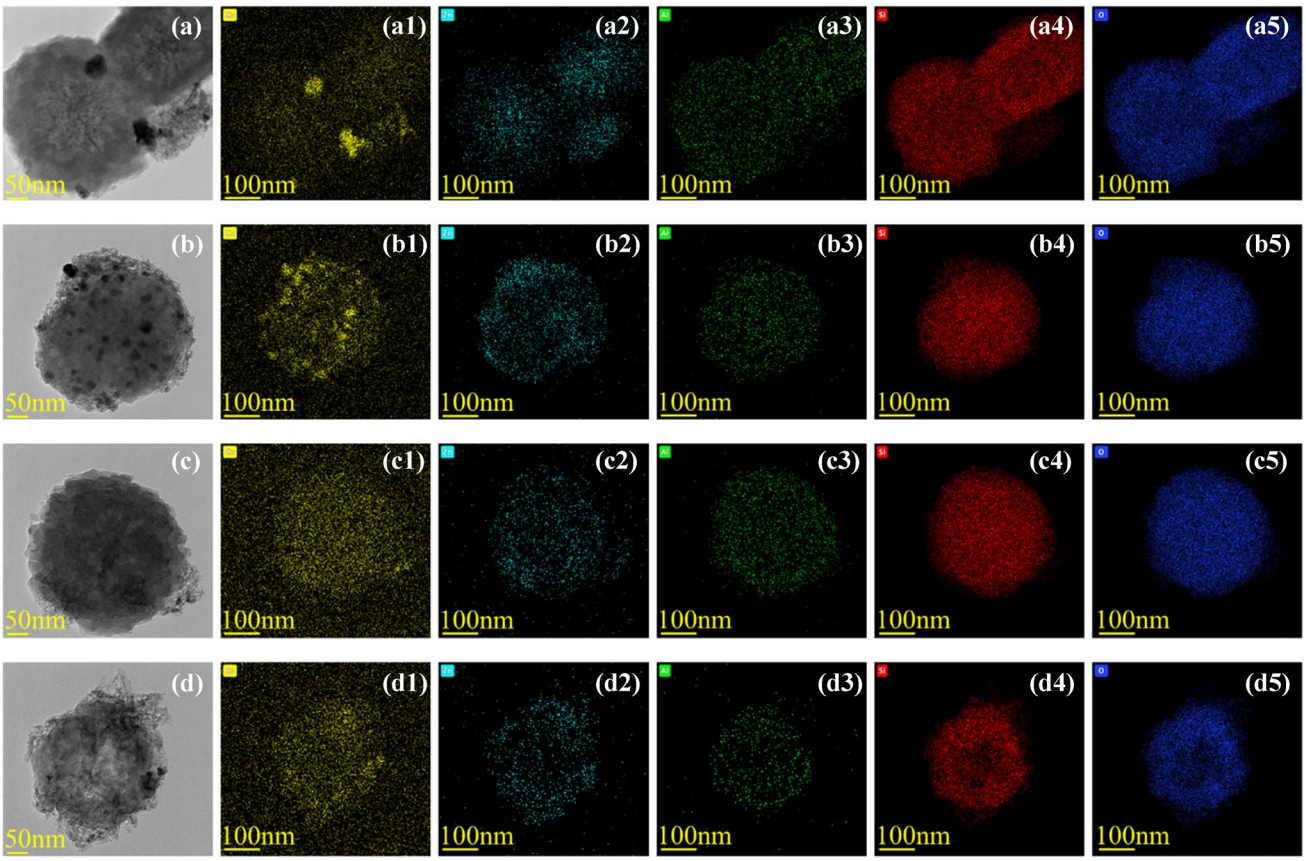

Fig. 5 TEM images and surface mapping of ASMZ catalysts: a TEM image of the ASMZ1 catalyst; b TEM image of the ASMZ2 catalyst; c TEM image of the ASMZ3 catalyst; d TEM image of the ASMZ4 catalyst; (1)~(5) surface mapping of the ASMZ catalysts: (1) Cu element; (2) Zn element; (3) Al element; (4) Si element; (5) O element

mapping of all catalysts. Among them, yellow is the Cu element distribution diagram of each catalyst, cyan is the Zn element distribution diagram of each catalyst, green is the Al element distribution diagram of each catalyst, red is the Si element distribution diagram of each catalyst, and blue is the O element distribution diagram of each catalyst. According to the test results, it can be found that the Si, O, and Al (from the CZA catalyst) elements of all catalysts are very evenly distributed on the zeolite. With the increase of the Si/Al ratio, the addition of CZA in ASMZ series catalysts gradually decreased, and the content of Cu element also decreased. According to the TEM surface scanning results of individual particles, it can be found that the distribution of Cu elements in the catalyst varies from large particles to small particles dispersed and further varies to very uniform. This verifies that the synthesis method in this study realizes the connection between ZSM-5 zeolite and CZA catalyst through the Al element to a certain extent. It is precisely because the ASMZ3 catalyst has the most uniform distribution of Cu elements, no agglomeration, and high content, its catalytic performance is the best.

Elemental state and valence analysis

In order to further understand the state of each element in the catalyst, the samples were analyzed by XPS. The XPS full spectrum analysis results of all catalysts are shown in Fig. S4. Fig. 6a shows the Al 2P of ASMZ3, CZA, and ZSM-5 catalysts.

The characteristic peaks for Al 2p founded at 75.4 and 78.0 eV of CZA were considered to be Al^{3+} present in Al_2O_3 species (Senthilkumar et al. 2021). The characteristic peak for Al 2P founded at 74.8 eV of ZSM-5 was considered to be Al atoms in the ZSM-5 framework, where Al atoms are connected to the bridged O atom in the –Si–O–Al–O– chains. Compared with CZA and ZSM-5 catalysts, the catalysts synthesized in this study additionally derived Al 2P with higher binding energy (~79.6). This observation shows that the aluminum atoms in ASMZ3, in addition to the two types mentioned above, form additional frames of alumina in very asymmetric and heterogeneous locations (twisted octahedrons) (Ali et al. 2014). This further proves that the experimental method in this paper realizes the connection between CZA catalyst and ZSM-5 zeolite through the Al

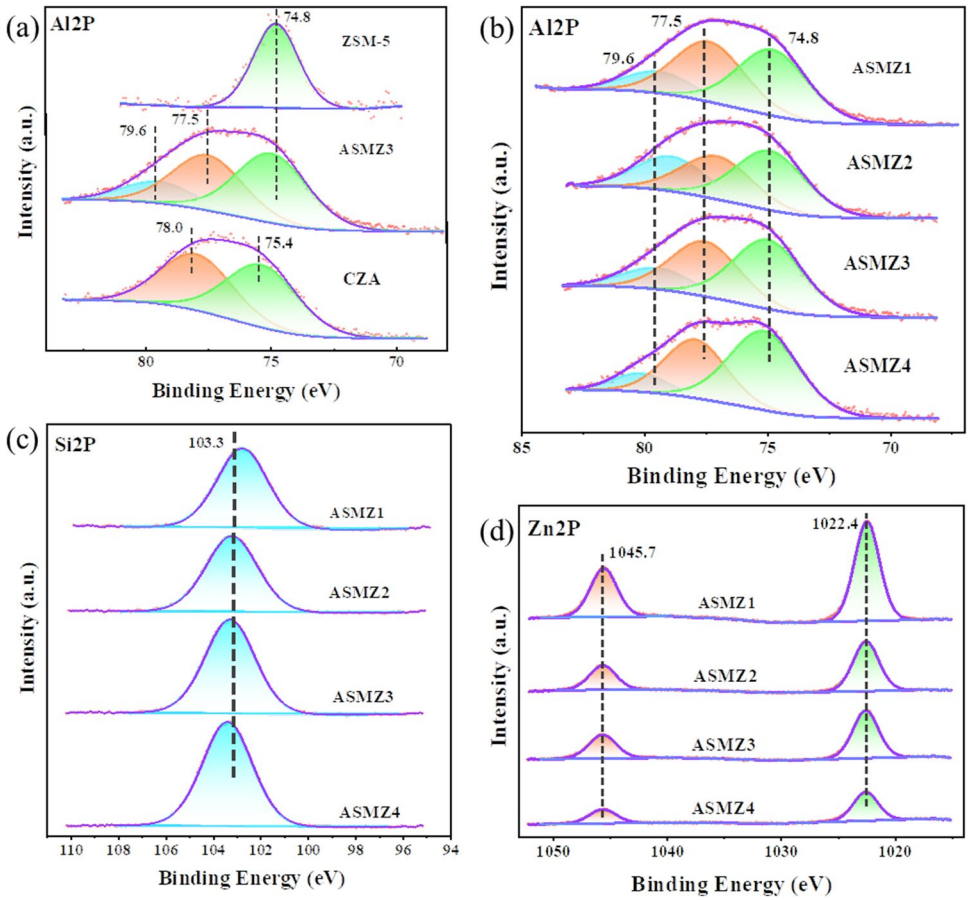

Fig. 6 XPS results: **a** Al 2P of ASMZ3, CZA, and ZSM-5 catalysts; **b** Al 2P of ASMZ catalysts; **c** Si 2P of ASMZ catalysts; **d** Zn 2P of ASMZ catalysts

element. Fig. 6b, c, d shows the fine spectra of the three elements Al, Si, and Zn in the ASMZ catalyst, respectively. Fig. 6b shows that all the catalysts contained three Al 2P characteristic peak at the binding energy of around 74.8, 77.5, and 79.6 eV. This means that each catalyst has to some extent achieved the connection of the ZSM-5 zeolite to the CZA by sharing the Al element. Fig. 6b shows that the Si 2P characteristic peak of each catalyst appears near the binding energy located at 103.3 eV, which is considered to be Si in the zeolite skeleton structure (Ojeda et al. 2018). Besides, as depicted in Fig. 6c, the evident peaks of binding energy located at around 1022.4 eV and 1045.7 eV can be ascribed to Zn 2p3/2 and Zn 2p1/2, respectively (Yang et al. 2018). The changing trend of Zn and Si element content is consistent with the added amount of raw materials. The results of XPS verify that the catalysts prepared in this study contain both CZA metal oxide and ZSM-5 zeolite structure, which is consistent with the characterization results of XRD. At the same time, XPS further verified the existence of the Al element connecting CZA and ZSM-5 zeolite in the catalyst and realized the close connection between the two, laying a foundation for the rapid transfer of catalytic products.

As the key active component of the catalytic CO_2 hydrogenation reaction, Cu's valence has the most direct influence on the reaction results. Therefore, the fine spectrum and Auger spectrum of Cu elements were further tested and analyzed in this study. Fig. 7a shows the results of the Cu 2p of ASMZ catalysts. The binding energies (BE) of Cu 2p3/2 and Cu 2p1/2 appear at around 933 eV and 953 eV, respectively. The presence of a shakeup satellite peak at about 944 eV reveals that the divalent copper (Cu^{2+}) is presented in catalysts (Xue et al. 2019). The shakeup satellite peak in the ASMZ1 catalyst is significantly higher than other catalysts, which is also because the proportion of CZA metal oxides in the ASMZ1 catalyst is the highest. A high proportion of CZA metal oxides were enriched and agglomerated in the catalyst, resulting in the inability of CuO to be completely oxidized to Cu^0 or Cu^{+1} under the reduction conditions in this study. The spectra of Cu 2p3/2 of all catalysts were deconvoluted into two peaks at around 932.9 eV and 935.1 eV. The spectra of Cu 2p1/2 of all catalysts were deconvoluted into two peaks at around 952.8 eV and 955.2 eV. However, Cu^0 and Cu^+ cannot be well distinguished by the Cu 2p spectrum due to their very close binding energies, and the X-ray induced Auger spectrum (XAES) of Cu LMM was hence adopted, in which the standard peaks of Cu^0 and Cu^+ are at approximately 916.8 and 913.8 eV, respectively. As can be observed in Fig. 7b, there is an obvious peak at 913.8

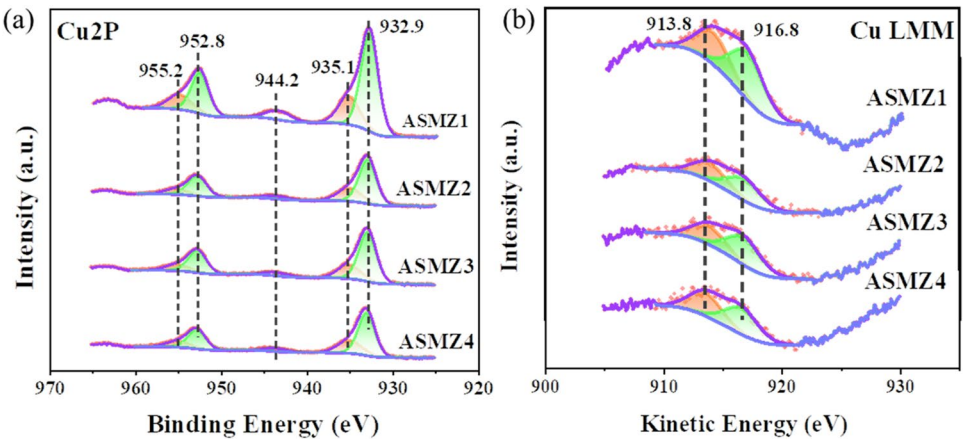

Fig. 7 **a** Cu 2P and **b** Cu LMM of ASMZ catalysts

eV (corresponding to Cu^{+}) for ASMZ catalysts, suggesting that copper mainly exists in the form of Cu^{+}. Although both Cu^{+} and Cu^{0} species are believed to the activity of Cu-based catalysts, a proper ratio of Cu^{+} and Cu^{0} is important for the catalytic performance in CO_2 hydrogenation to methanol (Li et al. 2020). Liu et al. (Liu et al. 2017) simulated and analyzed the mechanism of catalytic methanol synthesis at the Cu (111) and Cu_2O (111) interfaces by using DFT and concluded that CO_2 is the main carbon source on the Cu^{0} surface and CO is the main carbon source on the Cu^{+} surface. This further proves that the organic combination of Cu^{0} and Cu^{+1} is more conducive to the efficient CO_2 hydrogenation reaction (CO is the main intermediate product of the CO_2 hydrogenation reaction).

Catalyst surface active sites analysis

The reducibility of the active component Cu plays an important role in the catalytic reaction. Fig. 8a provides a detailed comparison of H_2-TPR test data for CZA, ZSM-5, and ASMZ3 catalysts. Since there is no active component Cu in the ZSM-5 zeolite, there is no obvious H_2 consumption peak during the testing process. The H_2 consumption peaks of CZA catalyst mainly occur at 231.8 and 259.9 °C. The H_2 consumption peak at 231.8 °C is considered a separate CuO reduction peak because it is the most easily reduced. The H_2 consumption peak of 259.9 °C is considered to be the CuO reduction characteristic peak combined with ZnO and Al_2O_3 (Fang et al. 2021). The H_2 consumption peak area of 259.9 °C accounts for 78.1% of the total peak area, indicating that most of the Cu in the CZA catalyst is combined with ZnO and Al_2O_3. In addition, when the temperature reaches 300 °C, the CuO in the CZA catalyst is basically completely reduced. Compared with the CZA catalyst, the H_2 consumption peaks of ASMZ catalysts shift to the direction of higher temperature. This is mainly due to the combination of some CuO in the CZA metal oxide with the ZSM-5 zeolite (Chen et al. 2016). In the ASMZ series of catalysts (Fig. 8b), CuO exists in two main situations: the situation of binding with ZnO and the situation of binding with the ZSM-5 zeolite (by binding with Al_2O_3). As the Si/Al ratio increases, the crystallinity of the ZSM-5 zeolite increases (according to XRD test results in Fig. 2a), and the corresponding proportion of CuO bound to the ZSM-5 zeolite also increases. All catalysts can be completely reduced at 300 °C, except for ASMZ1. This is mainly because the high CZA content in the ASMZ1 catalyst causes a large amount of CuO–ZnO–Al_2O_3 co-precipitate to agglomerate and accumulate on the zeolite

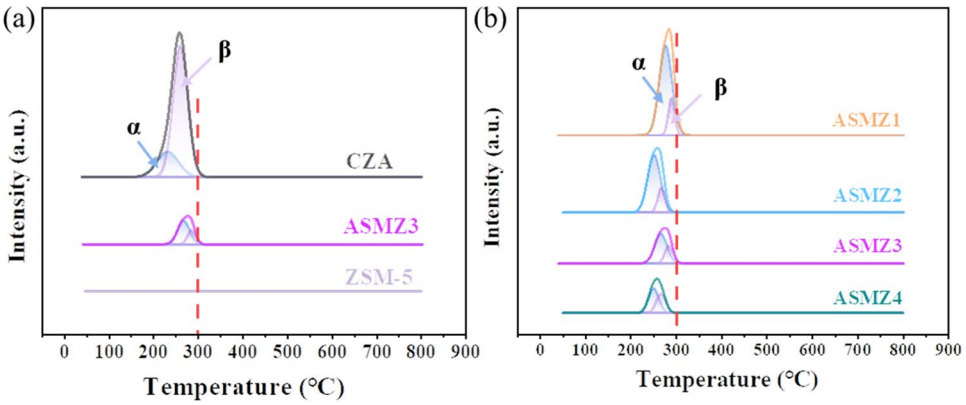

Fig. 8 H_2-TPR of **a** CZA, ZSM-5, and **b** ASMZ catalysts

surface, which increases the difficulty of reducing CuO in the catalyst, which is consistent with the scanning results of SEM. This also explains why there is a clear satellite peak in the Cu 2P test of the ASMZ1 catalyst (Table 3).

The strength and distribution of acidic sites in catalyst have an important influence on the CO_2 conversion and product distribution in the CO_2 hydrogenation reaction. Fig. 9 provides a detailed comparison of NH_3-TPD test data for CZA, ZSM-5, and ASMZ catalysts. In the CZA catalyst, almost no analytical peak of NH_3 exists, which means that there are almost no acidic sites in the catalyst. In the ZSM-5 zeolite, two typical NH_3 resolution peaks can be observed, at approximately 175 °C and 370 °C, respectively, for the desorption of NH_3 adsorbed at weakly acidic sites and at surface strongly acidic sites (Lou et al. 2016). It has been reported that the weak acid sites (Lewis acid sites) are correlated with the Si–OH in the H-ZSM-5 zeolite, whereas the strong acid sites (Brønsted acid sites) correspond to the protonic (Si–OH Al) (Zhu et al. 2021). In this study, CZA metal oxide was used as the aluminum source for the synthesis of the ZSM-5 zeolite, and the Al element not only formed proton Si–OH–Al in the zeolite skeleton, but also formed metal coprecipitate with CuO–ZnO. Therefore, the strong acid sites in ASMZ series catalysts were occupied, forming a large number of medium strength acid sites (Zhu et al. 2021). The weakly acidic site of Lewis acid carrier can promote the formation of CH_3OH, but the stronger acidic site can further catalyze the dehydration of CH_3OH to DME (Lam et al. 2019; Jiang et al. 2020). This also explains why the catalysts prepared in this study significantly improved the conversion rate of CO_2 and reduced the selectivity of CO in the product during the process of catalyzing CO_2 hydrogenation. It also explains why the reaction product is mainly methanol rather than DME. According to Fig. 9b, the acidic sites of ASMZ series catalysts first increased and then decreased with the increase of the Si/Al ratio, among which the weakly acidic sites of ASMZ3 were the most abundant. The low content of acidic sites in ASMZ1 and ASMZ2 is mainly due to the overcovering of large amounts of CZA metal oxides and the blockage of microchannels (Zhu et al. 2021). This is consistent with SEM results. In comparison, the CZA metal oxide content of the ASMZ3 catalyst is relatively appropriate, and the exposure of effective acidic sites in the catalyst is preserved to the greatest extent, while the number of acidic sites in the ASMZ4 catalyst is reduced due to the high Si/Al ratio.

Table 3 Partial peak fitting results of catalyst H_2-TPR test

Samples	Peak α (%)	Peak β (%)
CZA	21.9	78.1
ZSM-5	—	—
ASMZ1	82.8	17.2
ASMZ2	80.7	19.3
ASMZ3	71.5	28.5
ASMZ4	58.2	41.8

Peak α represents the H_2 consumption peak of the catalyst at lower temperature; Peak β represents the H_2 consumption peak of the catalyst at higher temperature

Catalytic mechanism analysis

After a series of characterization analysis, the catalytic mechanism of the catalyst in this study is inferred as shown in Fig. 10. In this study, the CZAB catalyst was prepared first, and CZABB was used as an aluminum source, and the characteristic that Al_2O_3 could be dissolved in alkaline solution was used to dissolve it in the TPAOH template agent, and then the HZSM-5 zeolite was prepared by a hydrothermal reaction. Thus, the catalysts prepared in this study mainly include the following reaction active sites: Cu^0/Cu^+, Cu–ZnO alloy interface, weak acid sites, medium strength acid sites, and strong acid sites. According to previous studies (Wang et al. 2019), the active sites for CO_2 adsorption and conversion are mainly Cu–ZnO alloy interface, and the active sites for H_2 adsorption and conversion are mainly Cu^+ and Cu^0. Under their catalytic action, CO_2 and H_2 produce two main products, methanol and CO (Yang et al. 2022). The two active sites are derived from the

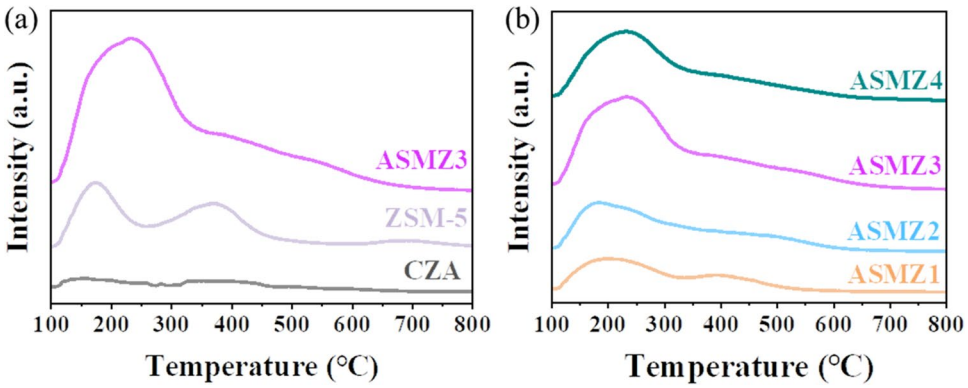

Fig. 9 NH_3-TPD of a CZA, ZSM-5, and b ASMZ catalysts

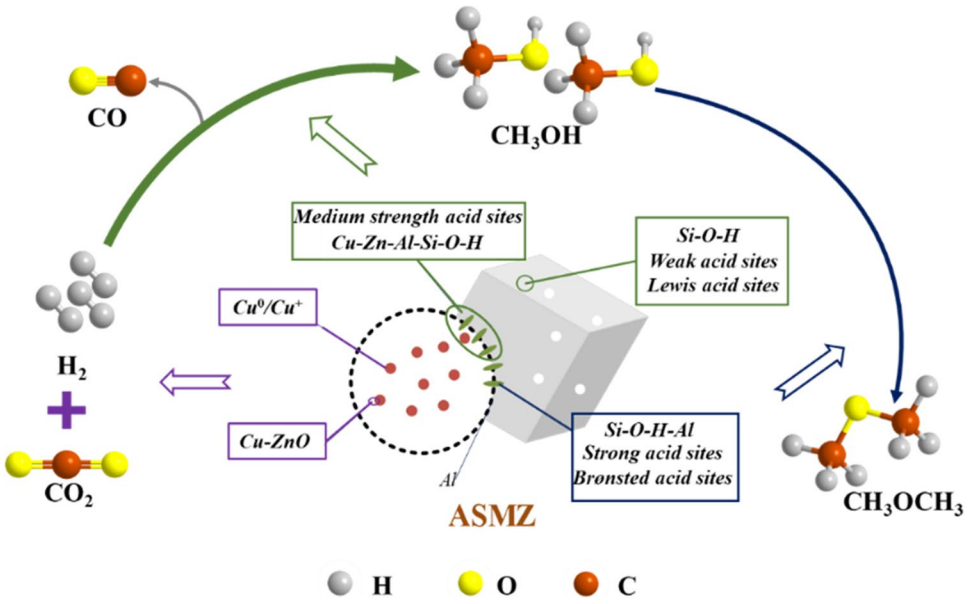

Fig. 10 Reaction mechanism diagram

CZAB catalyst prepared by coprecipitation and H_2 reduction treatment of ASMZ catalysts (Yang et al. 2021a). It is well known that there are usually two types of acidic sites in HZSM-5 zeolites: weakly acidic sites (Lewis acid sites) and strongly acidic sites (Brønsted acid sites). And the lower the Si/Al ratio, the higher the proportion of strongly acidic sites. The strong acidic site has a stronger dehydration ability, and it is easier to promote the dehydration of methanol to DME under the reaction conditions in this study. Because the concept of element sharing was applied to prepare the ASMZ catalyst in this study, the Al element not only formed proton Si–OH–Al in the molecular sieve skeleton, but also formed metal co-precipitation with CuO–ZnO, which led to the strong acid sites of ASMZ series catalysts being occupied, forming a large number of medium strong acid sites. This point is also verified by the characterization analysis of XPS and NH_3-TPD, and the presence of a large number of medium-strong acidic sites promotes the conversion of CO_2 hydrogenation to methanol. Therefore, the selectivity of CO in the reaction products is greatly reduced. In addition, the presence of a few strong acidic sites also promoted the dehydration of a small amount of methanol to DME. Based on the above analysis, the schematic diagram of the catalytic mechanism of ASMZ series catalysts is shown in Fig. 10.

In this study, by regulating the Si/Al ratio of the ZSM-5 zeolite and the ratio of zeolite to CZA metal oxide, it was found that the catalyst had the best performance when Si/Al was 30, which greatly improved the CO_2 conversion and methanol selectivity. This is mainly attributed to the following reasons: (1) Compared with ASMZ1 and ASMZ2, the distribution of CZA in the ASMZ3 catalyst is the most uniform, and there is no agglomeration of Cu elements (TEM test results), which ensures that the active component of ASMZ3 catalyst gives full play to its catalytic capacity; (2) Compared with catalysts ASMZ1 and ASMZ2, CZA largely covered the surface of the HZSM-5 zeolite and occupied its acidic sites, and the ASMZ3 catalyst retained the most medium-strong acidic sites (NH_3-TPD test results), which ensured that the catalyst promoted the conversion of CO_2 hydrogenation to methanol, and improved the CO_2 conversion rate and methanol selectivity. (3) Although the distribution of CZA in the ASMZ4 catalyst is also very uniform, its catalytic performance is slightly lower than that of the ASMZ3 catalyst due to the low content of active components and the small number of acidic sites.

Conclusions

In this study, ASMZ series catalysts were successfully prepared by means of element sharing. By adjusting the Si/Al ratio, it is found that the ASMZ3 catalyst has the highest CO_2 conversion (26.4%), the highest methanol selectivity (76.0%), and the lowest CO selectivity (15.3%) in this study. Through a series of characterization tests and analysis of the catalyst, it was found that the ASMZ catalyst prepared by this method significantly improved the CO_2 conversion and methanol selectivity compared with the traditional CZA catalyst, because the ZSM-5 zeolite introduced by this method contained a large number of weak acidic sites and medium strength acidic sites (which promoted the conversion of CO_2 hydrogenation to methanol). The appropriate ratio of CZA to ZSM-5 zeolite ensured the number of various acidic sites and the exposure of effective acidic sites. In addition, the close combination of CZA and ZSM-5 zeolite also ensured the timely transfer of

catalytic products and ensured that various catalytic active centers played a role in time to promote the reaction. The preparation method of the catalyst in this study also provides ideas for the preparation of catalysts for other uses.

Supplementary Information The online version contains supplementary material available at https://doi.org/10.1007/s11356-024-33959-7.

Author contribution All authors contributed to the study conception and design. Material preparation, data collection, and analysis were performed by He Jia, Tao Du, Yingnan Li, Heming Wang, Qiang Yue, Lifeng Zhou, and Yisong Wang. The first draft of the manuscript was written by He Jia, and all authors commented on previous versions of the manuscript. All authors read and approved the final manuscript.

The manuscript was written through contributions of all authors. All authors have given approval to the final version of the manuscript.

Funding This work was funded by the National Natural Science Foundation of China (No. 52270177), the Natural Science Foundation of Shenyang (No. 22-315-6-13), the Chunhui Project from the Ministry of Education of China (No. HZKY20220436), the Natural Science Foundation of Liaoning Province (No. 2023-MSBA-111), the 111 Project (No. B16009), and the Fundamental Research Funds for the Central Universities (No. N2325018).

The authors declare that no funds, grants, or other support were received during the preparation of this manuscript.

Declarations

Ethical approval Not applicable.

Consent to participate Not applicable.

Consent for publication Not applicable.

Competing interests The authors declare no competing interests.

References

Ahmed HE, Rashed AE, El-Khouly ME et al (2023) Green approach for sustainable production of paraffin fuel from CO_2 hydrogenation on Fe-MOF catalyst. J Environ Chem Eng 11. https://doi.org/10.1016/j.jece.2023.111071

Ali IO, El-Molla SA, Ibraheem IA, Salama TM (2014) Synthesis and characterization of metal oxides loaded-HZSM-5 and their implication for selective conversion of isopropanol. Micropor Mesopor Mater 197:48–57. https://doi.org/10.1016/j.micromeso.2014.05.039

Chen BH, Chao ZS, He H et al (2016) Towards a full understanding of the nature of Ni(II) species and hydroxyl groups over highly siliceous HZSM-5 zeolite supported nickel catalysts prepared by a deposition-precipitation method. Dalton Trans 45:2720–2739. https://doi.org/10.1039/c4dt00399c

Chen C, Song G, Wang Z et al (2024a) Insight into the synergistic effect of copper and sodium over metal organic framework-derived Fe-based catalyst for CO_2 hydrogenation to aromatics. Appl Catal B 341. https://doi.org/10.1016/j.apcatb.2023.123330

Chen G, Ma J, Gong W et al (2023) Recent progress of heterogeneous catalysts for transfer hydrogenation under the background of carbon neutrality. Nanoscale. https://doi.org/10.1039/D3NR05207A

Chen H, Cui H, Lv Y et al (2022) CO_2 hydrogenation to methanol over Cu/ZnO/ZrO_2 catalysts: effects of ZnO morphology and oxygen vacancy. Fuel 314. https://doi.org/10.1016/j.fuel.2021.123035

Chen Q, Meng S, Liu R et al (2024b) Plasma-catalytic CO_2 hydrogenation to methanol over CuO-MgO/Beta catalyst with high selectivity. Appl Catal B 342. https://doi.org/10.1016/j.apcatb.2023.123422

Ding X, Liu X, Cheng J et al (2024) Boosted photothermal synergistic CO_2 methanation over Ru doped Ni/ZrO_2 catalyst: from experimental to DFT studies. Fuel 357. https://doi.org/10.1016/j.fuel.2023.129779

Energy agency international (2022) CO_2 Emissions in 2022. https://www.iea.org/reports/co2-emissions-in-2022

Fang L, Huang T, Lu H et al (2023) Biochar-based materials in environmental pollutant elimination, H_2 production and CO_2 capture applications. Biochar 5(1):–42

Fang X, Men Y, Wu F et al (2021) Highly dispersed Cu-ZnO-ZrO_2 nanoparticles on hydrotalcite adsorbent as efficient composite catalysts for CO_2 hydrogenation to methanol. Korean J Chem Eng 38:747–755. https://doi.org/10.1007/s11814-020-0736-6

Guo Q, Li S, Li J et al (2021) Enhanced CO_2 hydrogenation to methanol on the mesostructured Cu-ZnO/Al_2O_3-ZrO_2 catalyst. ACS Appl Energy Mater 4:8311–8321. https://doi.org/10.1021/acsaem.1c01542

Jia H, Du T, Fang X et al (2021) Synthesis of template-free ZSM-5 from rice husk ash at low temperatures and its CO_2 adsorption performance. ACS Omega 6:3961–3972. https://doi.org/10.1021/acsomega.0c05842

Jiang Q, Liu Y, Dintzer T et al (2020) Tuning the highly dispersed metallic Cu species via manipulating Brønsted acid sites of mesoporous aluminosilicate support for CO_2 hydrogenation reactions. Appl Catal B 269. https://doi.org/10.1016/j.apcatb.2020.118804

Lam E, Corral-Pérez JJ, Larmier K et al (2019) CO_2 hydrogenation on Cu/Al_2O_3 : role of the metal/support interface in driving activity and selectivity of a bifunctional catalyst. Angewandte Chemie 131:14127–14134. https://doi.org/10.1002/ange.201908060

Li H, Xiao Y, Xiao J et al (2023) Selective hydrogenation of CO_2 into dimethyl ether over hydrophobic and gallium-modified copper catalysts. Chinese J Catal 54:178–187. https://doi.org/10.1016/S1872-2067(23)64535-8

Li S, Guo L, Ishihara T (2020) Hydrogenation of CO_2 to methanol over Cu/AlCeO catalyst. Catal Today 339:352–361. https://doi.org/10.1016/j.cattod.2019.01.015

Liu YM, Liu JT, Liu SZ et al (2017) Reaction mechanisms of methanol synthesis from CO/CO_2 hydrogenation on Cu_2O(111): comparison with Cu(111). J CO2 Util 20:59–65. https://doi.org/10.1016/j.jcou.2017.05.005

Lou Y, Ma J, Hu W et al (2016) Low-temperature methane combustion over Pd/H-ZSM-5: active Pd sites with specific electronic properties modulated by acidic sites of H-ZSM-5. ACS Catal 6:8127–8139. https://doi.org/10.1021/acscatal.6b01801

Ojeda M, Osterman N, Dražić G et al (2018) Conversion of palmitic acid over bi-functional Ni/ZSM-5 catalyst: effect of stoichiometric Ni/Al molar ratio. Top Catal 61:1757–1768. https://doi.org/10.1007/s11244-018-1046-7

Qi T, Li W, Li H et al (2021) Yttria-doped Cu/ZnO catalyst with excellent performance for CO_2 hydrogenation to methanol. Mol Catal 509. https://doi.org/10.1016/j.mcat.2021.111641

Ren S, Fan X, Shang Z et al (2020) Enhanced catalytic performance of Zr modified CuO/ZnO/Al_2O_3 catalyst for methanol and DME synthesis via CO_2 hydrogenation. J CO2 Util 36:82–95. https://doi.org/10.1016/j.jcou.2019.11.013

Ren S, Shoemaker WR, Wang X et al (2019) Highly active and selective Cu-ZnO based catalyst for methanol and dimethyl ether

synthesis via CO_2 hydrogenation. Fuel 239:1125–1133. https://doi.org/10.1016/j.fuel.2018.11.105

Senthilkumar S, Zhong W, Natarajan M et al (2021) A green approach for aerobic oxidation of benzylic alcohols catalysed by CuI-Y zeolite/TEMPO in ethanol without additional additives. New J Chem 45:705–713. https://doi.org/10.1039/d0nj03776a

Singh R, Tripathi K, Pant KK, Parikh JK (2022) Unravelling synergetic interaction over tandem Cu-ZnO-ZrO2/hierarchical ZSM5 catalyst for CO_2 hydrogenation to methanol and DME. Fuel 318. https://doi.org/10.1016/j.fuel.2022.123641

Sun Y, Liu X, Zhu M et al (2023) Non-noble metal single atom-based catalysts for electrochemical reduction of CO_2: synthesis approaches and performance evaluation. DeCarbon 2:100018. https://doi.org/10.1016/j.decarb.2023.100018

Wan Z, Wu W, Li G et al (2016) Effect of SiO_2/Al_2O_3 ratio on the performance of nanocrystal ZSM-5 zeolite catalysts in methanol to gasoline conversion. Appl Catal A Gen 523:312–320. https://doi.org/10.1016/j.apcata.2016.05.032

Wang G, Zuo Y, Han M, Wang J (2011) Cu-Zr-Zn catalysts for methanol synthesis in a fluidized bed reactor. Appl Catal A Gen 394:281–286. https://doi.org/10.1016/j.apcata.2011.01.010

Wang X, Alabsi MH, Zheng P et al (2022) PdCu supported on dendritic mesoporous $CexZr1\text{-}xO_2$ as superior catalysts to boost CO_2 hydrogenation to methanol. J Colloid Interface Sci 611:739–751. https://doi.org/10.1016/j.jcis.2021.11.172

Wang Y, Kattel S, Gao W et al (2019) Exploring the ternary interactions in Cu–ZnO–ZrO_2 catalysts for efficient CO_2 hydrogenation to methanol. Nat Commun 10. https://doi.org/10.1038/s41467-019-09072-6

Wang Y, Liu S, Wang J et al (2024) Direct conversion of carbon dioxide into light olefins over $ZnZrO_x$/ZSM-5@n-ZrO_2 tandem catalyst. Fuel 357. https://doi.org/10.1016/j.fuel.2023.129727

Xian Zhang; Xiaoliang Yang; Xi Lu (2023) China's carbon dioxide capture, utilization and storage (CCUS) annual report (2023). https://max.book118.com/html/2023/0713/5142303233010242.shtm

Xue H, Meng T, Liu F et al (2019) Enhanced resistance to calcium poisoning on Zr-modified Cu/ZSM-5 catalysts for the selective catalytic reduction of NO with NH_3. RSC Adv 9:38477–38485. https://doi.org/10.1039/c9ra07722g

Yang H, Liu Y, Liu X et al (2022) Large-scale synthesis of N-doped carbon capsules supporting atomically dispersed iron for efficient oxygen reduction reaction electrocatalysis. eScience 2:227–234. https://doi.org/10.1016/j.esci.2022.02.005

Yang H, Wang X, Zheng T et al (2021a) CrN-encapsulated hollow Cr-N-C capsules boosting oxygen reduction catalysis in PEMFC. CCS Chem 3:208–218. https://doi.org/10.31635/ccschem.020.202000645

Yang M, Yu J, Tong X et al (2021b) Flame-made Cu/ZrO_2 catalysts with metastable phase and strengthened interactions for CO_2 hydrogenation to methanol. Chem Commun 57:7509–7512. https://doi.org/10.1039/d1cc02784k

Yang X, Meng Q, Ding G et al (2018) Construction of novel Cu/ZnO-Al_2O_3 composites for furfural hydrogenation: the role of Al components. Appl Catal A Gen 561:78–86. https://doi.org/10.1016/j.apcata.2018.04.005

Zhang C, Wang L, Etim UJ et al (2022) Oxygen vacancies in Cu/TiO_2 boost strong metal-support interaction and CO_2 hydrogenation to methanol. J Catal 413:284–296. https://doi.org/10.1016/j.jcat.2022.06.026

Zhao Y, He D, Chen D et al (2020) Investigating the support effect for catalytic elimination of methyl mercaptan: role of hydroxyl groups over Cr-based catalysts. Catal Lett 150:2763–2773. https://doi.org/10.1007/s10562-020-03178-z

Zhu D, Wang Z, Meng F et al (2021) Catalytic conversion of chloromethane to olefins and aromatics over zeolite catalysts. Catal Lett 151:1038–1048. https://doi.org/10.1007/s10562-020-03364-z